RESEARCH | Article in Press

VE-PTP-targeted RBC-hybrid lipid nanoparticles restore endothelial ANG1–Tie2 signaling in diabetic kidney disease

Jee-Yeon Ryu · Geon Woo Baek · Nicholas J. Steers · Ilhwan Ryu · Jinsun Lee · Ara Ko · Sehoon Park · Dong Ki Kim

Received: 15 May 2026 / Accepted: 3 September 2026
© The Author(s) 2026

Abstract

Background Targeted delivery to injured glomerular endothelial cells remains a major challenge in diabetic kidney disease (DKD) because systemically administered therapeutics are limited by rapid kidney clearance, complex glomerular vascular architecture, and limited endothelial retention. Biomimetic red blood cell (RBC) membrane-hybrid lipid nanoparticles offer a promising strategy to improve vascular compatibility, prolong circulation, and protect therapeutic cargos. However, the application of this biomimetic platform for glomerular endothelial cell-targeted delivery of dCas9-based CRISPR activation (CRISPRa) ribonucleoprotein (RNP) complexes has not been established.

Results dCas9-sgRNA RNP complexes were efficiently incorporated into RBC-hybrid lipid nanoparticles through charge-mediated assembly using an ionizable lipid. The resulting VE-PTP-targeted RBC/LNP-Ab nanoparticles showed stable nanoscale size, favorable surface charge modulation, efficient RNP loading, and structural features consistent with RBC membrane-hybrid nanoparticle formation. In VE-PTP-upregulated endothelial cells under DKD-mimicking conditions, the nanoparticles enhanced intracellular dCas9 delivery and increased endogenous ANG1 expression, restoring the ANG1/ANG2 balance and downstream Tie2-Akt signaling. Following systemic administration in advanced DKD mice, VE-PTP-targeted RBC-hybrid nanoparticles preferentially localized to glomerular endothelial cells, increased ANG1 expression in the diabetic kidney, reduced albuminuria, and attenuated structural kidney injury.

Conclusions These results demonstrate that VE-PTP-targeted RBC-hybrid nanoparticles can serve as a biomimetic non-viral platform for glomerular endothelial cell-targeted CRISPRa RNP delivery. This strategy provides proof-of-concept for disease-specific transcriptional gene modulation in DKD and may provide a framework for targeted endothelial therapy in other microvascular diseases.

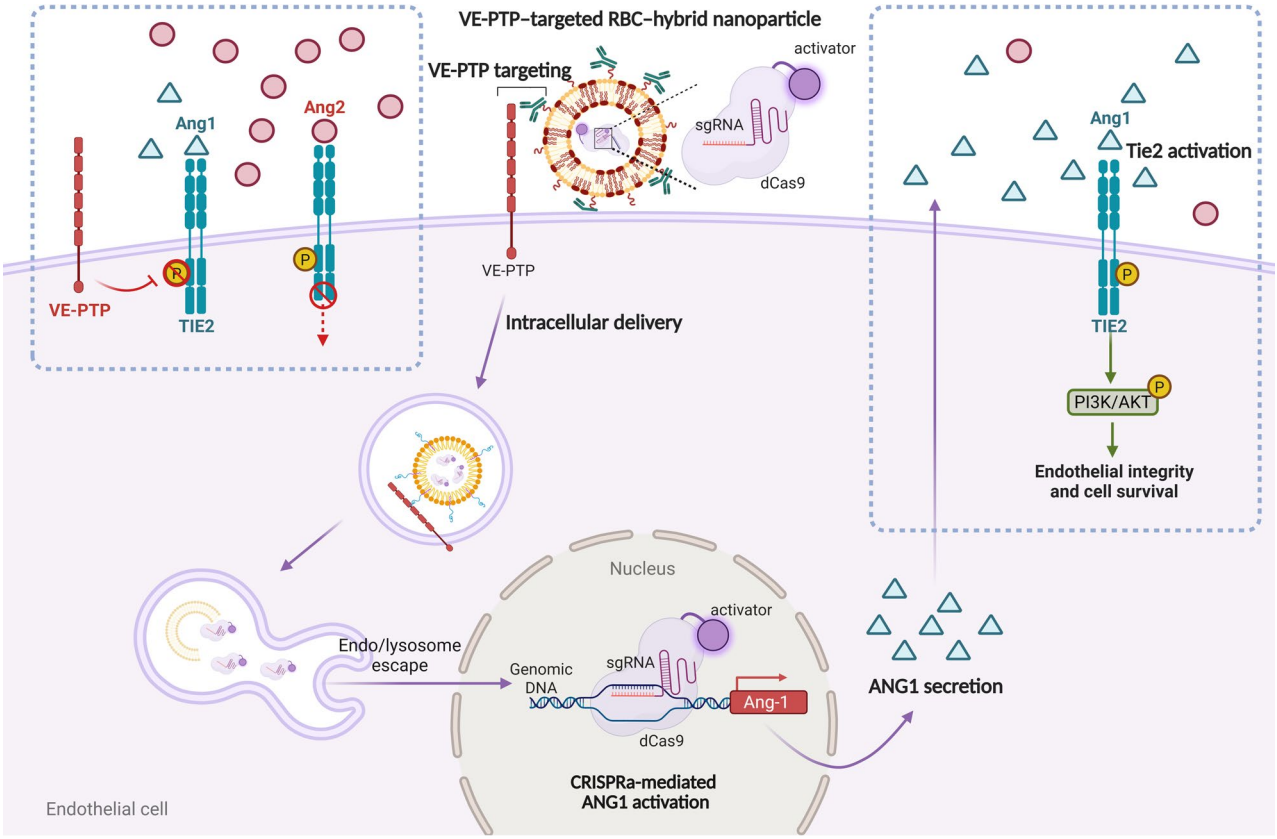
This Article in Press is shared early to give you faster access to new research. It is citable and carries a permanent DOI. The final edited version will replace it automatically.

Jee-Yeon Ryu, Geon Woo Baek and Nicholas J. Steers contributed equally to this work.

https://doi.org/10.1186/s12951-026-05042-5

Published online: 15 September 2026

Graphical abstract



Keywords RBC membrane-hybrid nanoparticles · dCas9 RNP delivery · Endothelial targeting · Diabetic kidney disease · ANG1-Tie2 signaling

Background

Diabetic kidney disease (DKD) is a leading cause of end-stage kidney disease worldwide [1, 2]. Glomerular endothelial cell (GEC) injury is increasingly recognized as an early event in DKD pathogenesis [3, 4]. Endothelial dysfunction contributes to albuminuria, microvascular rarefaction, and progressive fibrotic remodeling [5, 6]. However, therapeutic delivery to injured GECs remains challenging because rapid kidney filtration, complex glomerular vascular architecture, and limited endothelial retention restrict the accumulation of systemically administered therapeutics within the glomerulus.

Biomimetic membrane-hybrid nanoparticles provide a promising strategy to overcome these biological delivery barriers. Red blood cell (RBC) membranes provide a biomimetic interface that can improve vascular compatibility and support interactions with the endothelial surface [7, 8], whereas lipid nanoparticles (LNPs) provide a versatile core for encapsulating nucleic acid- or protein-based cargos [9, 10]. By integrating RBC membrane-derived biomimicry with LNP-mediated cargo loading, RBC membrane-hybrid LNPs may enhance vascular compatibility while supporting intracellular delivery. Surface functionalization with disease-relevant ligands can further enable targeted accumulation in pathological endothelial microenvironments [11, 12].

The angiopoietin (ANG)-TEK receptor tyrosine kinase (Tie2) signaling axis is a central regulator of glomerular vascular stability [13, 14]. Under diabetic conditions, decreased ANG1 expression shifts the ANG1-to-ANG2 balance toward endothelial destabilization, resulting in impaired Tie2 phosphorylation, weakened endothelial

junctions, and increased endothelial apoptosis [15–17]. Vascular endothelial protein tyrosine phosphatase (VE-PTP), a negative regulator of Tie2 signaling, is upregulated in injured GECs and further suppresses Tie2 activation [12, 14]. Thus, VE-PTP not only contributes to endothelial dysfunction but also provides a disease-associated molecular target for active delivery to injured glomerular endothelium.

In this study, we developed VE-PTP-targeted RBC membrane-hybrid lipid nanoparticles for glomerular endothelial delivery of dCas9-based CRISPR activation (CRISPRa) RNPs to reactivate endogenous ANG1 expression in DKD. The platform was designed to incorporate dCas9-sgRNA RNPs within LNPs, integrate the RNP-loaded LNPs with RBC membranes to generate a biomimetic hybrid structure, and functionalize the surface with anti-VE-PTP antibodies to target injured GECs. Using ANG1 as a therapeutic gene target, we investigated whether this biomimetic non-viral delivery platform could restore ANG1-Tie2 signaling and attenuate diabetic kidney injury.

Methods

In vitro transcription of sgRNAs and purification of the dCas9-VP64 protein

sgRNAs targeting the promoter regions of *ANG1* were designed using CRISPR activation design tools from MIT Feng Zhang Lab and further validated using CHOPCHOP and CRISPOR [18, 19]. The candidate ANG1-targeting sgRNA sequences were sgRNA1: GGGAGGGCCATACATGATCG, sgRNA2: GGCGGGATCGTCTTACAAA T, sgRNA3: ATGAGTGTGCCCCTATACTA. sgRNAs were synthesized by in vitro transcription using T7 RNA polymerase from dsDNA templates containing the protospacer and tracrRNA sequences. Following transcription, template DNA was removed by DNase I treatment and sgRNAs were purified by phenol-chloroform extraction. Predicted off-target loci for the ANG1-targeting sgRNA were identified using CRISPOR. The on-target sgRNA sequence and predicted off-target sequences are provided in Additional file 1: Figure S12a. Because the top-ranked off-target sites were located in intergenic regions, neighboring annotated genes, including GOLGA8S, SCRT2, and SLC52A3, were selected for targeted qPCR analysis.

For dCas9-VP64 protein production, His-tagged dCas9-VP64 plasmids were expressed in *Escherichia coli* following IPTG induction. Proteins were purified using Ni-NTA affinity chromatography, dialyzed into storage buffer, and quantified by BCA assay. To assemble CRISPR activation RNP complexes, purified dCas9-VP64 protein was mixed with sgRNAs at a 1:3 molar ratio and incubated at room temperature prior to downstream applications.

Preparation of dCas9-ANG1@RBC/LNP-Ab

RBC membranes were prepared from whole blood by sequential centrifugation, PBS washing, and hypotonic lysis to obtain RBC ghosts, followed by repeated washing until complete hemoglobin removal (Fig. 1b**)**. Purified membranes were stored in deionized water at 4 °C until use.

dCas9-ANG1-loaded LNPs were prepared using a lipid mixture composed of L-α-phosphatidylcholine, cholesterol, ALC-0315, DSPE-PEG(2000)-COOH, and PEG2000-PE. Lipid films were formed by solvent evaporation, hydrated with PBS containing preassembled dCas9-sgRNA RNP complexes, and processed by freeze-thaw cycles and probe sonication to generate RNP-encapsulated nanoparticles.

For fabrication of RBC membrane-hybrid nanoparticles, purified RBC membranes were combined with LNPs by probe sonication to facilitate structural integration and hybrid assembly. To achieve endothelial targeting, anti-VE-PTP antibodies were conjugated to DSPE-PEG(2000)-COOH on the nanoparticle surface using EDC/NHS chemistry. Excess antibodies were removed by centrifugation and washing. The resulting VE-PTP-functionalized RBC/LNP hybrid nanoparticles were used for subsequent experiments. For fluorescence tracking, nanoparticles were labeled with FITC, and unbound dye was removed by repeated washing and centrifugation.

https://doi.org/10.1186/s12951-026-05042-5

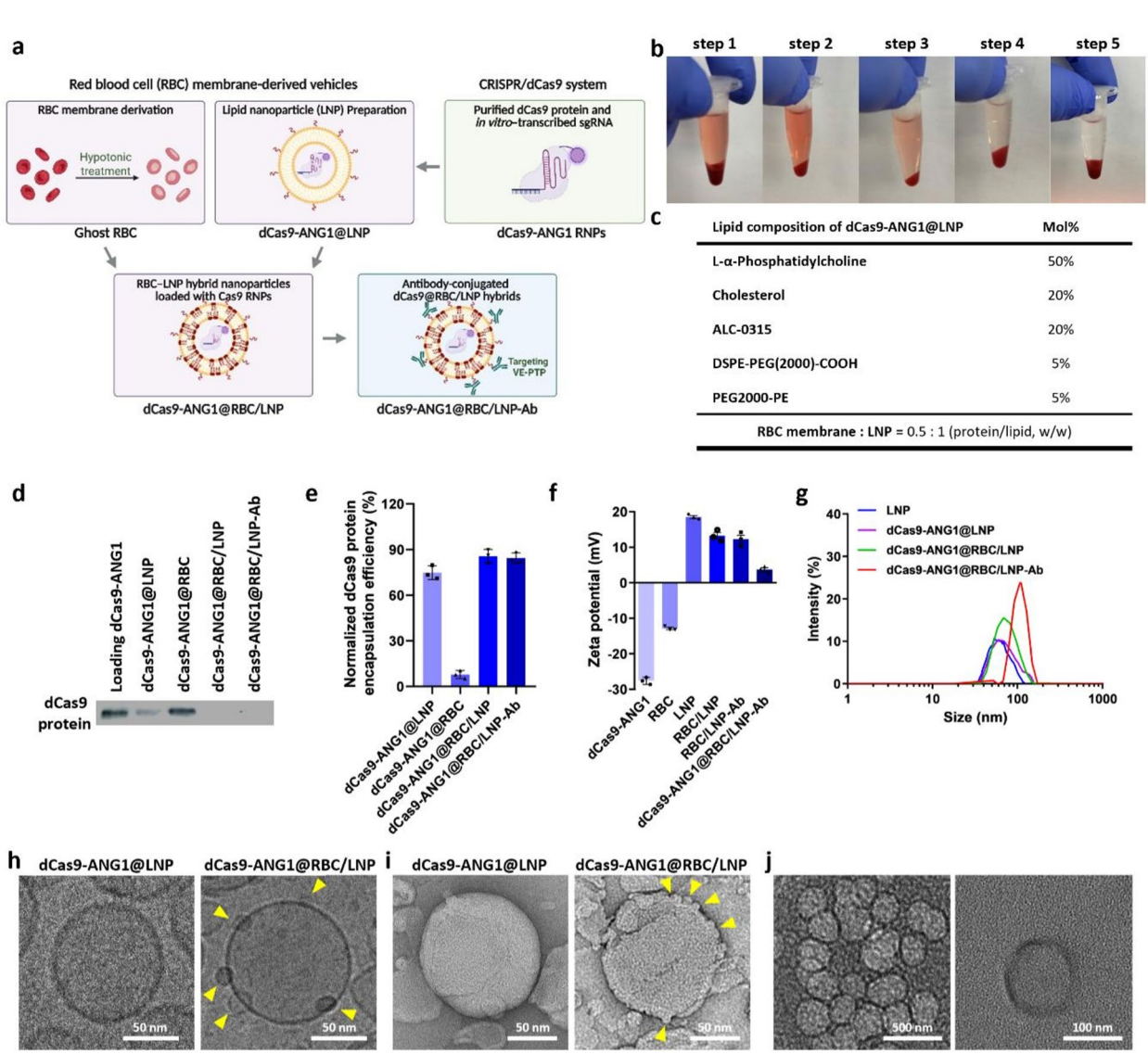


Fig. 1 Preparation and physicochemical characterization of VE-PTP-targeted biomimetic RBC membrane-hybrid lipid nanoparticles. (**a**) Schematic illustration of the fabrication of dCas9-ANG1 RNP-loaded RBC/LNP hybrid nanoparticles and subsequent VE-PTP antibody conjugation. (**b**) Representative images of RBC ghost preparation through stepwise hypotonic lysis. (**c**) Optimized lipid composition of the LNP core and RBC membrane-to-LNP fusion ratio. (**d**) Western blot analysis of dCas9 protein remaining in the supernatant after nanoparticle assembly. (**e**) Quantification of dCas9 encapsulation efficiency in the indicated formulations. (**f**) Zeta potential measurements showing surface charge changes during nanoparticle assembly. (**g**) Hydrodynamic size distribution of the indicated formulations measured by DLS. (**h**) Representative cryo-TEM images of dCas9-ANG1@LNP and dCas9-ANG1@RBC/LNP. Arrowheads indicate electron-dense membrane-associated domains along the nanoparticle periphery, consistent with incorporation of RBC membrane-derived components into the LNP surface. (**i**) Representative staining TEM images of dCas9-ANG1@LNP and dCas9-ANG1@RBC/LNP. Arrowheads indicate membrane-associated structures along the nanoparticle periphery. (**j**) Representative TEM images showing nanoscale morphology and size distribution of dCas9-ANG1@RBC/LNP-Ab nanoparticles. Data are presented as mean ± SD ($n = 3$). Figure 1a was created with BioRender.com

Characterization of the nanoparticles

Hydrodynamic size distribution and zeta potential were measured by dynamic light scattering (DLS) using a Zetasizer Nano ZS (Malvern Instruments, UK). Samples were diluted in PBS and measured at 25 °C. The morphology and structure of the nanoparticles were examined by transmission electron microscopy (TEM). A drop of nanoparticle suspension was placed onto a carbon-coated copper grid and allowed to adsorb for 1–2 min. Excess solution was removed with filter paper. The grids were air-dried and imaged using a transmission electron microscope operated at an accelerating voltage of 80–120 kV. For cryo-TEM analysis, nanoparticle suspensions were applied to glow-discharged holey carbon grids, blotted to remove excess liquid, rapidly vitrified in liquid ethane, and imaged under cryogenic conditions using a TEM. For negative-staining TEM, nanoparticle samples were placed on carbon-coated copper grids, stained with uranyl acetate or phosphotungstic acid, air-dried, and imaged by TEM. Scale bars are indicated in each figure.

Serum stability was evaluated by incubating dCas9-ANG1@RBC/LNP-Ab nanoparticles in PBS containing 10% FBS at 37 °C. At predetermined time points, hydrodynamic diameter and PDI were measured by DLS. Storage stability was assessed by storing nanoparticles in PBS at 4 °C, followed by measurement of hydrodynamic diameter, PDI, and zeta potential at days 0, 1, 3, 7, and 14. To evaluate dCas9 RNP release kinetics, dCas9-ANG1@RBC/LNP-Ab nanoparticles were incubated in buffer at pH 7.4 or pH 5.5 at 37 °C. At predetermined time points, samples were centrifuged to separate released dCas9 RNPs from nanoparticle-associated dCas9 RNPs. Cumulative release was calculated as the percentage of released dCas9 relative to the total encapsulated dCas9 protein.

Cell culture and co-culture

Human umbilical vein endothelial cells (HUVECs) were cultured in Dulbecco's modified Eagle's medium (DMEM, Gibco) supplemented with 10% fetal bovine serum (FBS) and 1% penicillin-streptomycin. Human kidney podocytes were maintained in epithelial cell medium (EpiCM, Innoport) supplemented with 2% FBS, 1% epithelial cell growth supplement, and 1% penicillin-streptomycin. All cells were incubated at 37 °C in a humidified atmosphere containing 5% CO_2. For glucose stimulation experiments, HUVECs were cultured under low-glucose (LG, 5.5 mM D-glucose) or high-glucose (HG, 30 mM D-glucose) conditions for 48 h. For hypoxic stimulation, cells were treated with cobalt chloride ($CoCl_2$) at a final concentration of 200 μM for 24 h to induce chemical hypoxia. Control cells were maintained under normoxic conditions without $CoCl_2$ treatment.

For co-culture experiments, HUVECs were seeded onto transwell inserts (0.4 μm pore size) and allowed to attach for 24 h. Cells were then treated with dCas9-ANG1@RBC/LNP-Ab for 2 h under HG conditions, with or without $CoCl_2$ treatment as indicated. The inserts containing HUVECs were subsequently transferred into wells containing podocytes seeded in the lower chamber. Co-culture was maintained for an additional 24 h before downstream analyses.

Human glomerular endothelial cells (hGECs) were cultured in endothelial cell growth medium supplemented with endothelial growth factors, fetal bovine serum, and antibiotics according to the supplier's instructions. For DKD-mimicking conditions, hGECs were exposed to high glucose and chemical hypoxia as described above. For VE-PTP blocking experiments, hGECs were pretreated with free anti-VE-PTP antibody before nanoparticle exposure. Nanoparticle uptake was analyzed by fluorescence imaging and flow cytometry. For ANG1 blockade experiments, anti-ANG1 neutralizing antibody was added during the endothelial-podocyte co-culture assay as indicated.

Cell viability assay

To assess podocyte viability, human kidney podocytes were seeded into 96-well plates and maintained at 37 °C under 5% CO_2. For indirect co-culture experiments, HUVECs were first treated with the indicated nanoparticle

formulations. After treatment, the conditioned media from HUVEC cultures were collected and transferred to podocytes seeded in 96-well plates. Podocytes were then incubated with the HUVEC-conditioned media. Cell viability was analyzed using a water-soluble tetrazolium salt (WST-1) assay (Dogen) according to the manufacturer's instructions. Briefly, WST-1 solution was added to each well, and the cells were incubated at 37 °C for 30 min. Absorbance was measured at 450 nm using a microplate reader (BioTek), and viability was calculated relative to control groups.

Animal studies

Animals. All experiments were approved by the Institutional Animal Care and Use Committee of Seoul National University Hospital (SNUH) (No. 25-0100-S1A0), and were conducted in accordance with SNUH IACUC guidelines. Male C57BLKS/J-db/db mice were purchased and were housed in a 12 h light/dark cycle, temperature-controlled room. Male mice were used to reduce biological variability and to maintain consistency with our established db/db 5/6 Nx protocol. Sex as a biological variable was not directly examined in the present study. Animals were divided into groups in a randomized fashion, and experiments were performed in a blinded manner.

5/6 nephrectomy model. To induce advanced diabetic kidney injury, 5/6 nephrectomy (5/6 Nx) was performed in db/db mice (db/db 5/6 Nx). Briefly, mice were anesthetized with isoflurane, and the right kidney was completely removed. One week later, approximately two-thirds of the left kidney was surgically excised by removal of the upper and lower poles to achieve a total 5/6 reduction of kidney mass. Sham-operated mice underwent identical surgical procedures without removal of kidney tissue. After recovery, mice were monitored for body weight and general health status. The dCas9-ANG1@RBC/LNP-Ab nanoparticles or control formulations were administered via tail vein injection once at a dose of 6 μg/kg based on dCas9 protein in a total nanoparticle dosing volume of 200 μL per mouse after 5/6 Nx, and mice were followed for 7 weeks after treatment. The 6 μg/kg dCas9 protein dose was selected with reference to our previous Cas9 protein/RNP nanoparticle delivery studies [20, 21] and preliminary formulation feasibility testing. This dose was used as a single-dose proof-of-concept regimen to evaluate endothelial-targeted ANG1 activation while minimizing the total amount of exogenous protein administered. A formal in vivo dose-response study was not performed.

Mice were randomly allocated to experimental groups, cage locations were randomized, and treatment and measurement order was rotated among groups. Outcome assessment was performed in a blinded manner. Group sizes for each endpoint are indicated in the corresponding figure legends. Blood and urine samples were collected at predetermined intervals, and tissues were harvested at the study endpoint for histological, immunoblotting, and immunofluorescence analyses. Unless otherwise specified, analyses were performed using all available samples. Animals were excluded only for pre-defined reasons, including death before the planned endpoint, surgery-unrelated severe illness requiring humane euthanasia, or technically unsuitable samples. No animals were excluded based on outcome values. Mortality, when present, was recorded and included in survival analysis. Sample sizes were selected based on feasibility, prior experience with the db/db 5/6 Nx model, and expected effect sizes; no formal prospective power calculation was performed.

Immunofluorescence

For immunofluorescence staining of cultured cells, HUVECs, hGECs, or podocytes were seeded onto glass coverslips and treated under the indicated experimental conditions. Cells were washed with PBS, fixed with 4% paraformaldehyde for 15 min at room temperature, and permeabilized with 0.25% Triton X-100 in PBS for 10 min. After blocking with 1% bovine serum albumin (BSA) in PBS for 1 h, cells were incubated with primary antibodies overnight at 4 °C. For tissue staining, Optimal Cutting Temperature (OCT) compound (Leica)-embedded frozen kidney sections were fixed in ice-cold acetone for 15 min and permeabilized with 0.25% Triton X-100 in PBS for 10 min at room temperature. Sections were then blocked with 1% BSA for 2 h and incubated with primary antibodies overnight at 4 °C.

The following primary antibodies were used: anti-Cas9 (Cell Signaling Technology, Cat. No.14697), anti-VE-PTP (Invitrogen, Cat. No. MA5-32904), anti-ANG1 (Invitrogen, Cat. No. AF923), anti-ANG2 (Invitrogen, Cat. No. PA5-27297), anti-CD31 (Cell Signaling Technology, Cat. No. 77699) and anti-Podocin (Invitrogen, Cat. No. PA5-79757). Primary antibodies were used at dilutions ranging from 1:100 to 1:500, according to the manufacturer's recommendations and preliminary optimization. After washing three times with 0.25% Triton X-100 in PBS, samples were incubated with Alexa Fluor 488-, 594- or Alexa Fluor 647-conjugated secondary antibodies for 1 h in the dark. Nuclei were counterstained with DAPI-containing mounting medium (Abcam). Immunofluorescence images were acquired using a confocal laser scanning microscope (LSM 980, Zeiss) under identical imaging settings within each experiment. DAPI, FITC/Alexa Fluor 488, Cy3/Alexa Fluor 555, and Cy5/Alexa Fluor 647 signals were detected using 405, 488, 561, and 633/640 nm laser lines, respectively. Laser power, detector gain, exposure time, and image acquisition parameters were kept constant among groups for quantitative comparison. Scale bars are indicated in each figure.

Image analysis was performed using ImageJ. Mean fluorescence intensity was measured after background subtraction. Marker-positive areas were quantified using fixed threshold settings applied equally across groups within each experiment. Colocalized areas were quantified from merged binary masks and normalized to the indicated marker-positive or glomerular area.

RT-qPCR

Total RNA was extracted from harvested mouse tissues or cultured cells using TRIzol reagent (Invitrogen) according to the manufacturer's instructions. Briefly, samples were homogenized in TRIzol, and RNA was separated by chloroform extraction followed by isopropanol precipitation. The RNA pellet was washed with 70% ethanol, air-dried, and dissolved in RNase-free water. RNA concentration and purity were determined using a spectrophotometer. cDNA was synthesized from 1 μg of total RNA using the Maxima cDNA Synthesis Kit for RT-qPCR (Thermo Scientific) according to the manufacturer's protocol. Quantitative PCR was performed using SYBR Green Master Mix (Applied Biosystems) on the StepOnePlus Real-Time PCR System (Applied Biosystems). The thermal cycling conditions were as follows: initial denaturation at 95 °C for 4 min, followed by 40 cycles of denaturation at 95 °C for 20 s, annealing at 60 °C for 20 s, and extension at 72 °C for 15 s. A final extension step was performed at 72 °C for 20 s. Relative gene expression levels were calculated using the 2^-ΔΔCt method and normalized to the indicated housekeeping gene.

Western blot

Harvested cells and mouse tissues were lysed in RIPA Lysis and Extraction Buffer (Thermo Scientific) and protein concentration was measured using a BCA assay (Pierce). Total protein (20 μg per well) was separated by SDS-PAGE and transferred to a PVDF membrane. The membrane was incubated with antibodies: anti-Cas9 (Cell Signaling Technology, Cat. No. 14697), anti-VE-PTP(Invitrogen, Cat. No. MA5-32904), anti-ANG1(Invitrogen, Cat. No. PA1-32150), anti-ANG2(Invitrogen, Cat. No. PA5-27297), anti-CD47(Cell Signaling Technology, Cat. No. SC63000), anti-AE1/SLC4A1 (Cell Signaling Technology, Cat. No. 23276), anti-HIF1α (Cell Signaling Technology, Cat. No. 79233), anti-Akt (Cell Signaling Technology, Cat. No. 9272), anti-phospho-Akt (Cell Signaling Technology, Cat. No. 4060), anti-Tie2 (Cell Signaling Technology, Cat. No. 4224), anti-phospho Tie2 (Cell Signaling Technology, Cat. No. 4221), anti-FoxO1 (Cell Signaling Technology, Cat. No. 2880), and anti-phospho FoxO1 (Cell Signaling Technology, Cat. No. 9461). Primary antibodies were used at dilutions ranging from 1:1000 to 1:3000, according to the manufacturer's recommendations and preliminary optimization. The membrane was visualized using ImageQuant LAS 500 (GE Healthcare).

Kidney function and albuminuria assessment

Urine samples were collected from mice using metabolic cages for 24 h. Urinary albumin concentration was determined using a mouse-specific ELISA kit, and urinary creatinine was measured by a colorimetric assay. The urinary albumin-to-creatinine ratio (uACR) was calculated as the ratio of albumin to creatinine (μg/mg). Blood samples were collected via cardiac puncture, and blood urea nitrogen (BUN) levels were measured using a commercially available colorimetric assay kit.

Periodic Acid-Schiff (PAS) staining

Paraffin-embedded kidney sections were deparaffinized, rehydrated through graded ethanol, and rinsed in distilled water for 5 min. Sections were treated with 0.5% periodic acid solution for 5 min and then incubated with Schiff reagent for 10 min. Slides were washed in running tap water for 10 min to allow color development. Nuclei were counterstained with Harris hematoxylin for 5 min, followed by rinsing in water for 5 min. Differentiation was performed by dipping slides 3–4 times in 1% HCl alcohol, followed by gentle washing in running water. Sections were then dehydrated, cleared, and mounted with a permanent mounting medium. PAS staining was conducted using the Roche Ventana Benchmark automated staining platform with the Roche PAS staining kit, following the manufacturer's protocol.

Masson's Trichrome (MT) staining

Paraffin-embedded kidney sections were deparaffinized in xylene and rehydrated through a graded ethanol series, followed by rinsing in distilled water for 5 min. Sections were mordanted in Bouin's solution at 56 °C for 1 h and subsequently washed in running tap water for 10 min to remove excess picric acid. Nuclei were stained with Weigert's iron hematoxylin for 10 min and rinsed in running water for 10 min. Sections were then stained with Biebrich scarlet-acid fuchsin solution for 10–15 min, followed by differentiation in phosphotungstic acid-phosphomolybdic acid (PTA-PMA) solution for 5 min. After brief rinsing, sections were sensitized in 0.5% acetic acid for 10 min and stained with aniline blue solution for 5 min without additional washing steps. Slides were thoroughly rinsed in distilled water, dehydrated through graded alcohols, cleared in xylene, and mounted with a permanent mounting medium. Staining was performed using the Roche Ventana Benchmark automated staining system with the Roche Masson's Trichrome staining kit according to the manufacturer's instructions.

Statistical analysis

Data are presented as mean ± SD. Normality was assessed using the Shapiro-Wilk test. Statistical analyses were performed using GraphPad Prism. Differences between two groups were analyzed using Student's t-test, while comparisons among multiple groups were performed using one-way or two-way ANOVA followed by Tukey's post hoc test. For survival analysis, Kaplan-Meier survival curves were generated, and statistical differences between groups were evaluated using the Log-rank (Mantel-Cox) test.

Results

Preparation and characterization of VE-PTP-targeted RBC-hybrid nanoparticles for dCas9-ANG1 delivery

To achieve selective targeting and transcriptional activation of ANG1 in GECs, we engineered a biomimetic hybrid nanoparticle platform by integrating RBC membranes with synthetic LNPs loaded with nuclease-deficient

Cas9 (dCas9) RNP complexes (Fig. 1a). The construction of this hybrid platform was optimized by screening candidate sgRNAs targeting the *ANG1* promoter (Additional file 1: Figure S1a). Among three candidates, sgRNA2 exhibited the most potent induction at both mRNA (~ 10-fold) and protein levels and was selected as the lead candidate (Additional file 1: Figure S1b-c). Purified dCas9 protein was assembled with in vitro-transcribed sgRNA2 targeting the *ANG1* promoter to generate a functional RNP complex. This dCas9-sgRNA2 complex was subsequently incorporated into RBC-hybrid nanoparticles, enabling targeted delivery and transcriptional activation in endothelial cells.

RBC ghosts were prepared through repeated cycles of hypotonic lysis and subsequently fused with dCas9-loaded LNPs (Fig. 1b). Notably, both the dCas9-ANG1 RNP and RBC membrane were net negatively charged under the tested conditions, generating electrostatic repulsion that hinders stable association with the RBC membrane and reduces RNP loading efficiency in the dCas9-ANG1@RBC formulation (Fig. 1d-e). To improve RNP loading efficiency, incorporation of the ionizable cationic lipid ALC-0315 facilitated electrostatic interactions with negatively charged dCas9-ANG1 RNPs (Fig. 1c-f). This charge-mediated assembly partially neutralized the surface charge and enabled efficient encapsulation within the LNP core prior to RBC membrane hybrid assembly (Fig. 1f). Consequently, incorporation of the ionizable LNP core significantly improved RNP loading efficiency compared with dCas9-ANG1@RBC and promoted stable integration with the negatively charged RBC membrane fragments. The final dCas9-ANG1@RBC/LNP-Ab formulation showed an encapsulation efficiency of 85.0 ± 0.6% and a loading capacity of 16.15 ± 0.11 μg dCas9 per mg lipid, supporting efficient dCas9 RNP incorporation into the hybrid nanoparticle system (Additional file 1: Table S1). Comprehensive physicochemical characterization of all major formulations was further performed, including hydrodynamic diameter, polydispersity index (PDI), and zeta potential (Fig. 1g and Additional file 1: Table S2). RBC membrane fragments and dCas9-ANG1@RBC showed relatively large particle sizes and higher PDI values, indicating heterogeneous membrane-associated assemblies. In contrast, incorporation of the LNP core produced uniform nanoscale hybrid nanoparticles with markedly reduced PDI values. The final dCas9-ANG1@RBC/LNP-Ab formulation showed a hydrodynamic diameter of 115.0 ± 3.5 nm, a low PDI of 0.10 ± 0.01, and a mildly positive zeta potential of + 8.0 ± 1.0 mV, supporting stable and homogeneous nanoparticle assembly. To assess manufacturing reproducibility, three independent batches of the final dCas9-ANG1@RBC/LNP-Ab formulation were prepared and characterized. The hydrodynamic diameter, PDI, zeta potential, encapsulation efficiency, and loading capacity were highly consistent across batches, supporting reproducible nanoparticle assembly (Additional file 1: Table S3). The final dCas9-ANG1@RBC/LNP-Ab formulation maintained stable hydrodynamic size and PDI in 10% FBS-containing medium for 48 h and during storage at 4 °C for up to 14 days (Additional file 1: Figure S2a, b). In release kinetic studies, dCas9 release was limited under physiological pH 7.4 conditions but increased under acidic pH 5.5 conditions, supporting enhanced RNP release in an endosomal/lysosomal-like environment (Additional file 1: Figure S2c).

Incorporation of RBC membrane components into the hybrid nanoparticles was further supported by western blot analysis of CD47 and AE1/SLC4A1, representative RBC membrane-associated proteins [22]. Both CD47 and AE1 were retained in dCas9-ANG1@RBC/LNP and dCas9-ANG1@RBC/LNP-Ab, whereas these markers were absent or minimally detected in dCas9-ANG1@LNP, supporting preservation of RBC membrane components after nanoparticle assembly (Additional file 1: Figure S3). To further evaluate RBC membrane-hybrid nanoparticle formation, we performed cryo-TEM and staining TEM analyses. Compared with dCas9-ANG1@LNP, dCas9-ANG1@RBC/LNP showed additional membrane-associated domains intermittently distributed along the nanoparticle periphery, consistent with incorporation of RBC membrane-derived components into the LNP surface (Fig. 1h, i). TEM imaging further confirmed the nanoscale morphology and size distribution of the resulting dCas9-ANG1@RBC/LNP-Ab nanoparticles (Fig. 1j). These structural data support successful assembly of dCas9-ANG1@RBC/LNP hybrid nanoparticles.

To confer endothelial specificity, the hybrid nanoparticles were functionalized with carboxyl-terminated polyethylene glycol (PEG-COOH), which served as a linker for conjugation of antibodies against VE-PTP. In addition to providing sites for antibody attachment, PEGylation enhanced nanoparticle dispersion and colloidal stability

under physiological conditions. The conjugation efficiency of VE-PTP antibodies to generate the final dCas9-ANG1@RBC/LNP-Ab formulation was confirmed by western blot analysis, as indicated by minimal unbound antibodies in the supernatant (Additional file 1: Figure S4a). The 10:1 antibody/LNP ratio showed minimal residual unbound antibody, corresponding to an estimated conjugation efficiency of 98.6% and an estimated antibody loading of 9.9 μg anti-VE-PTP antibody per mg lipid (Additional file 1: Figure S4b). Based on this analysis, the 10:1 ratio was selected as the optimized conjugation condition for subsequent experiments. Physicochemical characteristics of the nanoparticle formulations, including dCas9-ANG1@LNP, dCas9-ANG1@RBC/LNP, and dCas9-ANG1@RBC/LNP-Ab, were systematically analyzed to confirm successful hybrid formation and structural integrity. DLS analysis demonstrated a stepwise increase in hydrodynamic diameter during nanoparticle assembly (Fig. 1g). TEM imaging further confirmed the nanoscale morphology and size distribution of dCas9-ANG1@RBC/LNP-Ab nanoparticles (Fig. 1j). The average particle size increased from approximately 80 nm for dCas9-ANG1@LNP to ~110 nm for dCas9-ANG1@RBC/LNP-Ab following RBC membrane integration and antibody conjugation.

Collectively, these results confirm that the engineered RBC-hybrid nanoparticles possess the structural integrity and enhanced RNP loading capacity required for endothelial-targeted gene activation. Importantly, the combination of ionizable lipid-mediated RNP encapsulation and RBC membrane integration addresses two major barriers in protein-based CRISPR delivery: inefficient loading of large RNP complexes and poor biological compatibility after systemic administration. Preservation of CD47 and AE1 further suggests that RBC membrane-derived "self" components were retained after hybrid nanoparticle assembly, supporting the biomimetic nature of the platform. Thus, the resulting dCas9-ANG1@RBC/LNP-Ab nanoparticles provide a structurally stable and biologically interfaced delivery system suitable for subsequent endothelial targeting studies.

Targeted gene activation and restored Tie2 signaling in endothelial cells under diabetic conditions

To evaluate the therapeutic potential of the dCas9-ANG1@RBC/LNP-Ab system, we established an in vitro diabetic condition by exposing HUVECs to high glucose (HG) and hypoxia. Hypoxic stimulation was validated by robust induction of HIF1α expression in both normal glucose (NG) and HG groups, as confirmed by quantitative RT-PCR and western blot analysis (Fig. 2a-b). Under combined HG and hypoxic conditions, ANG1 expression was significantly reduced, whereas VE-PTP expression was markedly increased, indicating a pathological shift toward Tie2 deactivation in endothelial cells (Fig. 2a-b). These findings demonstrate that the diabetic condition promotes decreased ANG1 and elevated VE-PTP expression. Accordingly, this pathological imbalance provides a strong rationale for simultaneously targeting VE-PTP and activating *ANG1* expression through gene editing as a therapeutic strategy in DKD.

To assess endothelial targeting, we next examined the cellular targeting of VE-PTP-targeted dCas9-ANG1@RBC/LNP-Ab nanoparticles in HUVECs by confocal laser scanning microscopy (CLSM) (Fig. 2c-d). Under control conditions, VE-PTP was localized along the endothelial cell membrane (Additional file 1: Figure S5a). In contrast, exposure to HG and hypoxia resulted in a marked increase in VE-PTP fluorescence intensity and a broader membrane distribution across the cell surface (Additional file 1: Figure S5b). Rather than being restricted to junctional sites, VE-PTP displayed a more diffuse and intensified membrane-associated pattern, suggesting that DKD conditions induce both upregulation and spatial redistribution of VE-PTP. Such redistribution may increase the accessibility of VE-PTP to Tie2, thereby facilitating Tie2 dephosphorylation and contributing to impaired endothelial signaling. Following nanoparticle treatment under diabetic conditions, CLSM revealed pronounced co-localization of dCas9-ANG1@RBC/LNP-Ab (red) with VE-PTP (green), supporting VE-PTP-associated endothelial targeting (Fig. 2c). To further compare intracellular delivery efficiency and VE-PTP-dependent targeting specificity, HUVECs were treated with different nanoparticle formulations under identical DKD conditions, and dCas9 localization was analyzed (Fig. 2d and Additional file 1: Figure S6). Notably, robust intracellular green fluorescence corresponding to dCas9 was observed predominantly in cells treated with dCas9-ANG1@RBC/LNP-Ab, whereas dCas9-ANG1@LNP, dCas9-ANG1@RBC/LNP, and the isotype IgG-conjugated control

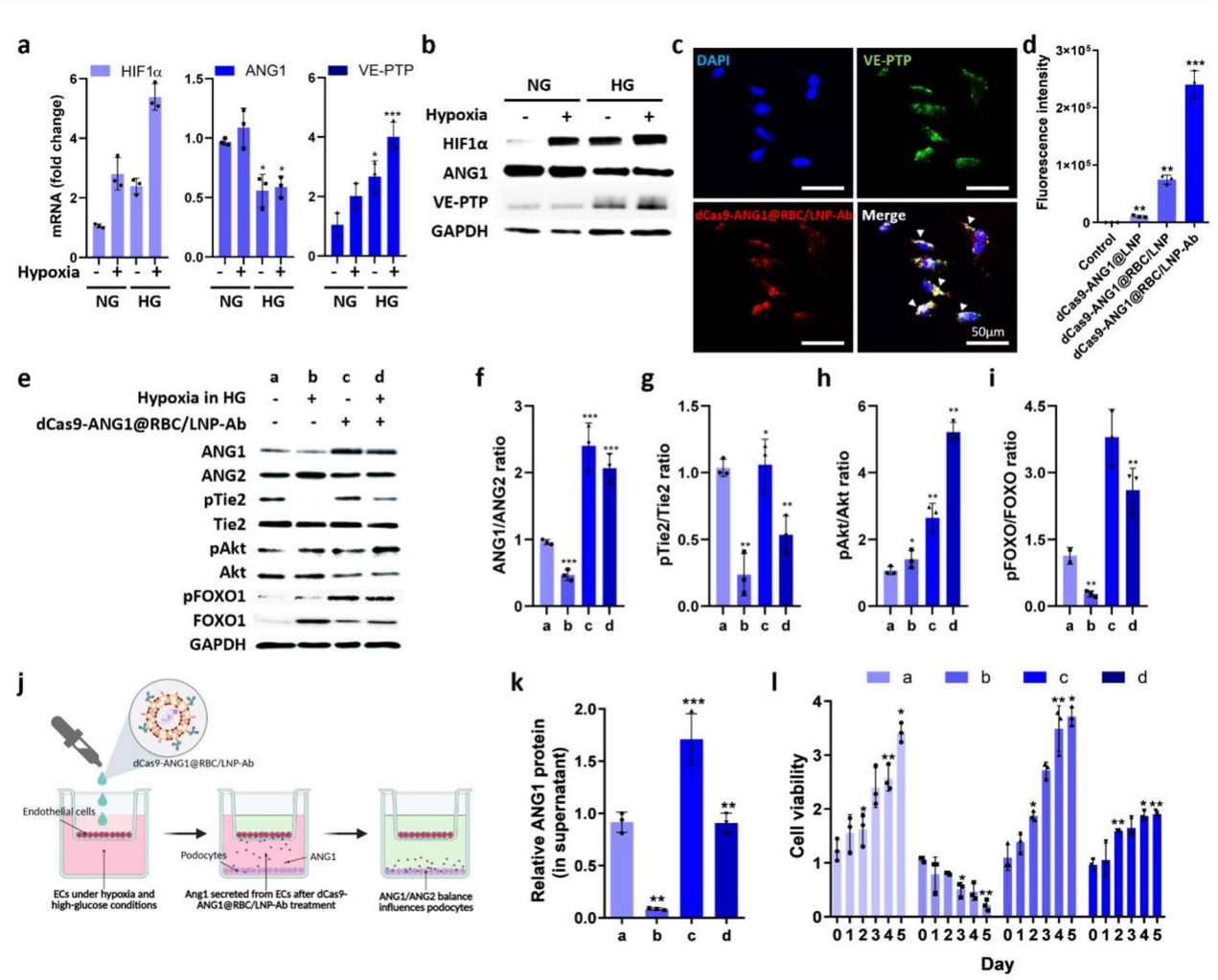


Fig. 2 In vitro validation of VE-PTP-directed dCas9 delivery and ANG1-Tie2 signaling restoration in endothelial cells. (**a**, **b**) mRNA and protein expression levels of HIF1α, ANG1, and VE-PTP in HUVECs exposed to high glucose (HG) and hypoxia. (**c**) CLSM images showing co-localization of dCas9-ANG1@RBC/LNP-Ab (red) with VE-PTP (green) on the HUVEC surface under DKD-mimicking conditions. (**d**) Quantification of intracellular dCas9 fluorescence intensity across different nanoparticle treatment groups. (**e-i**) Western blot analysis and quantification of ANG1-Tie2 pathway components, including phosphorylated Tie2, Akt, and FOXO1. (**j**) Schematic of the endothelial-podocyte co-culture system used to assess paracrine effects of endothelial ANG1 activation. (**k**) Secreted ANG1 protein levels in conditioned medium measured by western blot. (**l**) Podocyte viability in the co-culture system under DKD-mimicking conditions over 5 days. Data are presented as mean ± SD ($n = 3$); *$p < 0.05$, **$p < 0.01$, ***$p < 0.001$. Figure 2j was created with BioRender.com

formulation dCas9-ANG1@RBC/LNP-IgG exhibited markedly weaker signals. These results indicate that VE-PTP antibody functionalization, rather than nonspecific antibody conjugation, enhances dCas9 delivery into endothelial cells under DKD conditions.

To investigate the functional impact of dCas9-mediated ANG1 activation, cells were treated with dCas9-ANG1@RBC/LNP-Ab under diabetic conditions or normoxic control conditions. Cells treated with dCas9-ANG1@RBC/LNP-Ab effectively upregulated ANG1 expression, leading to a significant restoration of the ANG1/ANG2 ratio which had been disrupted by hypoxia (Fig. 2e-f). This restoration of ligand balance successfully reinvigorated the downstream signaling axis, as evidenced by the increased phosphorylation of Tie2 (pTie2) and Akt (pAkt) (Fig. 2e, g,h). Furthermore, we observed an increase in pFOXO1 levels, indicating that the activated Tie2 signaling successfully suppressed the nuclear translocation of FOXO1, a key transcriptional

driver of ANG2 expression (Fig. 2e, i). These results indicate that VE-PTP-targeted nanoparticles efficiently deliver dCas9 into endothelial cells under diabetic conditions, leading to robust ANG1 activation and restoration of the ANG1/ANG2 balance. This rebalanced ligand environment reactivated the Tie2-Akt signaling axis and suppressed FOXO1 nuclear translocation, indicating recovery of endothelial homeostasis.

To further determine whether the upregulated ANG1 was functionally secreted and capable of exerting paracrine effects, we performed a co-culture experiment with podocytes (Fig. 2j). This approach allowed us to evaluate whether endothelial ANG1 activation could influence neighboring podocyte responses within a DKD-mimicking microenvironment. Secreted ANG1 from nanoparticle-treated HUVECs significantly increased ANG1 protein levels in the medium (Fig. 2k and Additional file 1: Figure S7), even under a DKD-mimicking environment. This increased ANG1 availability resulted in improved podocyte viability under HG and hypoxia conditions (Fig. 2l), suggesting that endothelial-targeted ANG1 activation may influence neighboring podocytes through paracrine signaling within the glomerular microenvironment.

Collectively, these findings demonstrate that VE-PTP antibody functionalization enhances dCas9 RNP delivery to VE-PTP-upregulated endothelial cells under DKD-mimicking conditions. This result highlights the value of using a disease-induced endothelial marker as an active targeting cue for biomimetic nanocarriers. Beyond intracellular delivery, the platform achieved functional transcriptional modulation, as ANG1 activation restored the ANG1/ANG2 balance and downstream Tie2-Akt signaling. The co-culture results further suggest that endothelial-directed gene activation may influence neighboring podocytes, indicating that targeted modulation of GECs can affect the broader glomerular microenvironment.

Validation of VE-PTP-targeted dCas9-ANG1 delivery in human glomerular endothelial cells

We next examined whether the VE-PTP-targeted dCas9-ANG1 delivery platform remained effective in human glomerular endothelial cells (hGECs), a kidney-relevant endothelial model. Under high-glucose and hypoxic conditions, hGECs showed increased VE-PTP expression compared with control conditions, supporting the relevance of VE-PTP as a targeting marker in glomerular endothelial cells under DKD-mimicking stress (Fig. 3a). Consistent with this VE-PTP induction, treatment with dCas9-ANG1@RBC/LNP-Ab resulted in enhanced intracellular dCas9 signals in hGECs under high-glucose/hypoxic conditions (Fig. 3a). We further examined dCas9 localization in hGECs, as CRISPRa-mediated transcriptional activation requires nuclear access of dCas9. The encapsulated dCas9 protein contained a nuclear localization signal (NLS), which was designed to facilitate nuclear import after intracellular delivery. Consistently, dCas9 signals were detected within DAPI-positive nuclei following dCas9-ANG1@RBC/LNP-Ab treatment, supporting NLS-assisted nuclear delivery of dCas9 in target glomerular endothelial cells (Fig. 3b). We next assessed whether this delivery resulted in functional activation of the ANG1-Tie2 signaling axis. Western blot analysis showed that dCas9-ANG1@RBC/LNP-Ab increased ANG1 expression and restored downstream Tie2 signaling in hGECs under DKD-mimicking conditions, as indicated by increased phosphorylation of Tie2 and Akt (Fig. 3c).

To further determine whether nanoparticle uptake was mediated by VE-PTP-dependent targeting rather than nonspecific nanoparticle internalization, we performed VE-PTP blocking experiments. VE-PTP blockade reduced intracellular nanoparticle uptake in hGECs treated with dCas9-ANG1@RBC/LNP-Ab (Fig. 3d). Flow cytometric quantification further confirmed a decrease in FITC-positive hGECs following VE-PTP blockade, supporting VE-PTP-dependent uptake of the antibody-functionalized RBC/LNP nanoparticles (Fig. 3e).

Finally, we evaluated the functional consequences of endothelial ANG1 activation using an endothelial-podocyte co-culture system (Fig. 3f). hGECs were first treated with the indicated nanoparticle formulations under high-glucose/hypoxic conditions and were then co-cultured with podocytes to assess whether endothelial-derived factors affected podocyte function. Under high-glucose/hypoxic conditions, migratory capacity was impaired in both hGECs and co-cultured podocytes. Treatment of hGECs with dCas9-ANG1@RBC/LNP-Ab restored hGEC migration and improved podocyte migration, suggesting that ANG1 activation in endothelial cells exerted a protective paracrine effect on podocytes. This recovery was attenuated by VE-PTP blockade, which competes

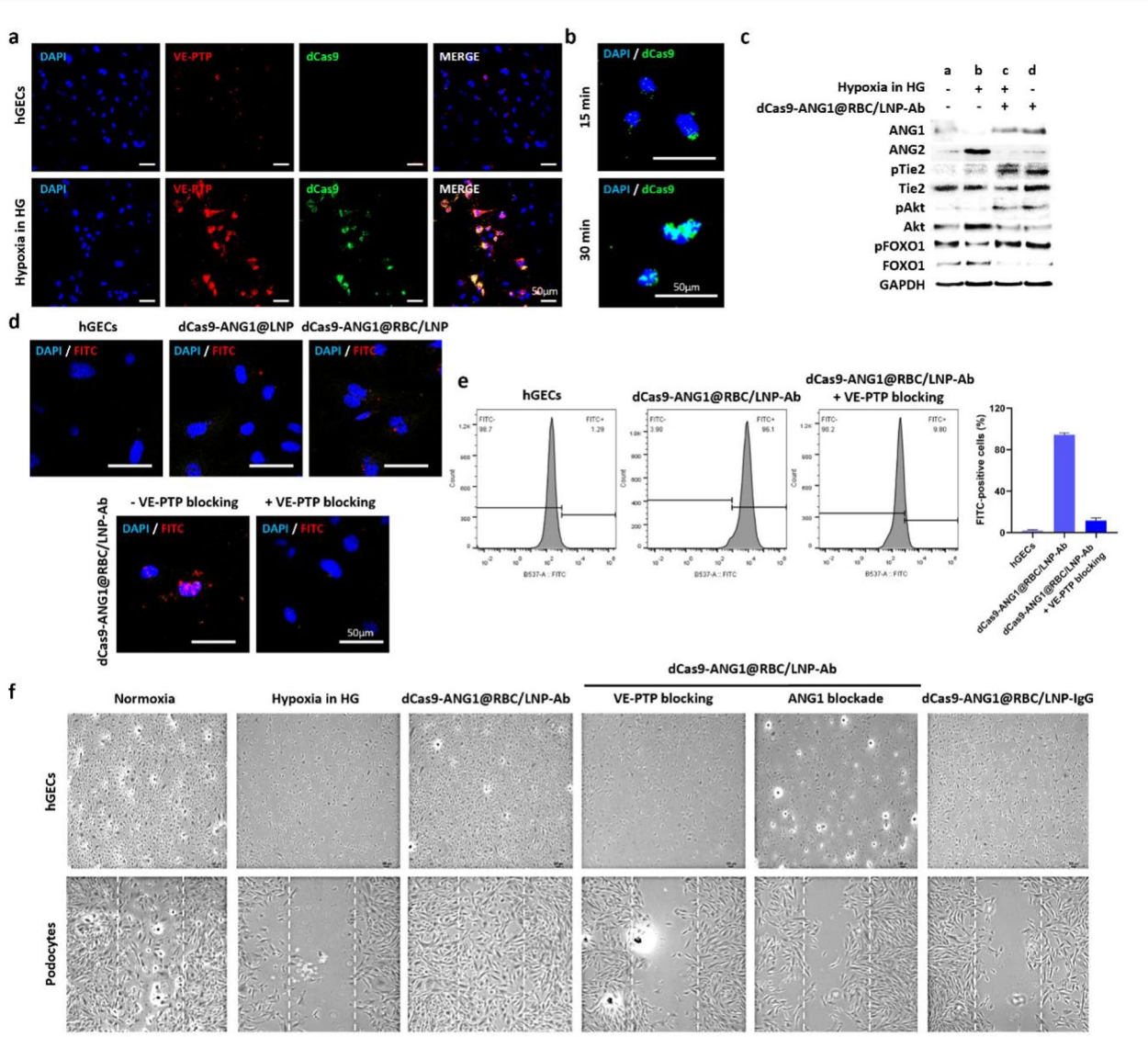


Fig. 3 Validation of VE-PTP-targeted dCas9-ANG1 delivery in human glomerular endothelial cells. (**a**) Representative immunofluorescence images showing VE-PTP expression and dCas9 uptake in human glomerular endothelial cells (hGECs) under DKD-mimicking conditions. (**b**) Representative images showing nuclear localization of dCas9 in DAPI-positive hGEC nuclei after dCas9-ANG1@RBC/LNP-Ab treatment. (**c**) Western blot analysis of ANG1-Tie2 signaling components in hGECs under the indicated conditions. (**d**, **e**) Representative fluorescence images and flow cytometric quantification of nanoparticle uptake in hGECs with or without VE-PTP blocking. (**f**) Quantification of migration in hGECs and podocytes under the indicated co-culture conditions. Data are presented as mean ± SD ($n = 3$)

with VE-PTP antibody-mediated nanoparticle binding to hGECs, and by ANG1 blockade, which neutralizes endothelial-derived ANG1 in the conditioned medium. In addition, isotype IgG-conjugated nanoparticles failed to rescue podocyte migration, consistent with reduced hGEC targeting in the absence of VE-PTP antibody functionalization (Fig. 3f). These findings support that VE-PTP-targeted dCas9-ANG1 delivery restores endothelial ANG1 signaling and promotes endothelial-podocyte functional protection through ANG1-dependent paracrine signaling in a kidney-relevant co-culture model.

Targeted delivery of dCas9-ANG1@RBC/LNP-Ab restores ANG1-Tie2 signaling in vivo

To evaluate in vivo targeting efficiency and therapeutic gene activation, we employed a db/db mouse model combined with 5/6 nephrectomy (5/6 Nx) to induce advanced diabetic kidney injury characterized by severe endothelial dysfunction and disruption of the ANG1-Tie2 axis (Fig. 4a) [23, 24]. This model recapitulates the progressive decline in endothelial stability and heightened VE-PTP expression observed in advanced DKD. Following systemic administration, whole-body fluorescence imaging demonstrated that dCas9-ANG1@RBC/LNP-Ab exhibited markedly enhanced kidney accumulation compared with LNP-only (dCas9-ANG1@LNP) or non-targeted RBC-hybrid (dCas9-ANG1@RBC/LNP) formulations (Fig. 4b and Additional file 1: Figure S8). Ex vivo organ imaging further supported preferential kidney localization of the antibody-conjugated hybrid nanoparticles. Quantification of organ-associated Cas9 fluorescence at 72 h revealed that, among non-kidney organs, residual fluorescence was detected mainly in the liver, while other examined organs showed relatively low signal levels (Additional file 1: Figure S9a). Although fluorescence imaging at 2 h post-injection suggested early liver accumulation, ANG1 expression levels in major organs, including the liver, remained unchanged at 3 days post-treatment, indicating the absence of off-target transcriptional activation (Additional file 1: Figure S9b). In contrast, ANG1 expression was increased in the kidney, indicating that early biodistribution to the liver did not translate into sustained or functional gene activation. These findings demonstrate that VE-PTP-mediated targeting enables kidney-preferential functional ANG1 activation despite transient systemic distribution.

Immunofluorescence analysis of kidney sections using FITC-labeled nanoparticles demonstrated prominent glomerular localization of dCas9-ANG1@RBC/LNP-Ab in treated mice, with substantial overlap between FITC signals and the endothelial marker CD31 (Fig. 4c). In contrast, nanoparticles lacking VE-PTP antibody functionalization showed weaker localization within CD31-positive glomerular endothelial regions, supporting the targeting specificity of the antibody-conjugated RBC-hybrid nanoparticle platform (Fig. 4d). Quantitative analysis further confirmed increased FITC/CD31 colocalized area in the dCas9-ANG1@RBC/LNP-Ab-treated group, indicating preferential accumulation of the nanoparticles in glomerular endothelial regions in vivo (Fig. 4e). To further assess potential off-target localization within kidney compartments, kidney sections were co-stained with nephrin, PDGFRβ, and AQP1, markers of podocytes, mesangial cells, and proximal tubular epithelial cells, respectively. FITC-labeled dCas9-ANG1@RBC/LNP-Ab nanoparticles showed substantially higher colocalization with CD31-positive glomerular endothelial cells than with nephrin-positive podocytes, PDGFRβ-positive mesangial cells, or AQP1-positive proximal tubules (Fig. 4f, g). These results support preferential glomerular endothelial localization of the VE-PTP-targeted formulation in vivo.

We next examined whether endothelial-targeted ANG1 activation restored the disrupted ANG1-Tie2 signaling axis. In db/db sham and db/db 5/6 Nx mice (groups b and c), ANG1 expression was markedly reduced, whereas ANG2 and VE-PTP levels were significantly elevated compared with db/m controls (group a), reflecting a pathological shift toward Tie2 inactivation (Fig. 5a, b). Treatment with dCas9-ANG1@RBC/LNP-Ab (group d) significantly increased ANG1 expression at both mRNA and protein levels while concomitantly suppressing ANG2 and VE-PTP expression in diabetic kidney tissues (Fig. 5c, d). To clarify the duration of ANG1 activation after a single injection, we performed a time-course analysis of kidney ANG1 expression following systemic administration of dCas9-ANG1@RBC/LNP-Ab. ANG1 mRNA increased after treatment, peaked at day 3, and gradually declined by day 14 while remaining higher than DKD control levels (Additional file 1: Figure S10a). Consistently, ANG1 protein expression showed a similar temporal pattern, with increased expression after treatment followed by gradual attenuation over time (Additional file 1: Figure S10b). These results indicate that a single injection of dCas9-ANG1@RBC/LNP-Ab induces transient but sustained ANG1 activation in the kidney.

This coordinated modulation rebalanced the ANG1/ANG2 ratio and reduced the abundance of the endogenous Tie2 phosphatase VE-PTP. Consistent with ligand rebalancing, restoration of downstream signaling was observed. Western blot analysis demonstrated increased phosphorylation of Tie2 and Akt in the treatment group compared with untreated db/db 5/6 Nx mice (Fig. 5d, e). Furthermore, phosphorylation of FOXO1 was enhanced, suggesting reduced nuclear activity of this transcription factor and subsequent suppression of ANG2 expression.

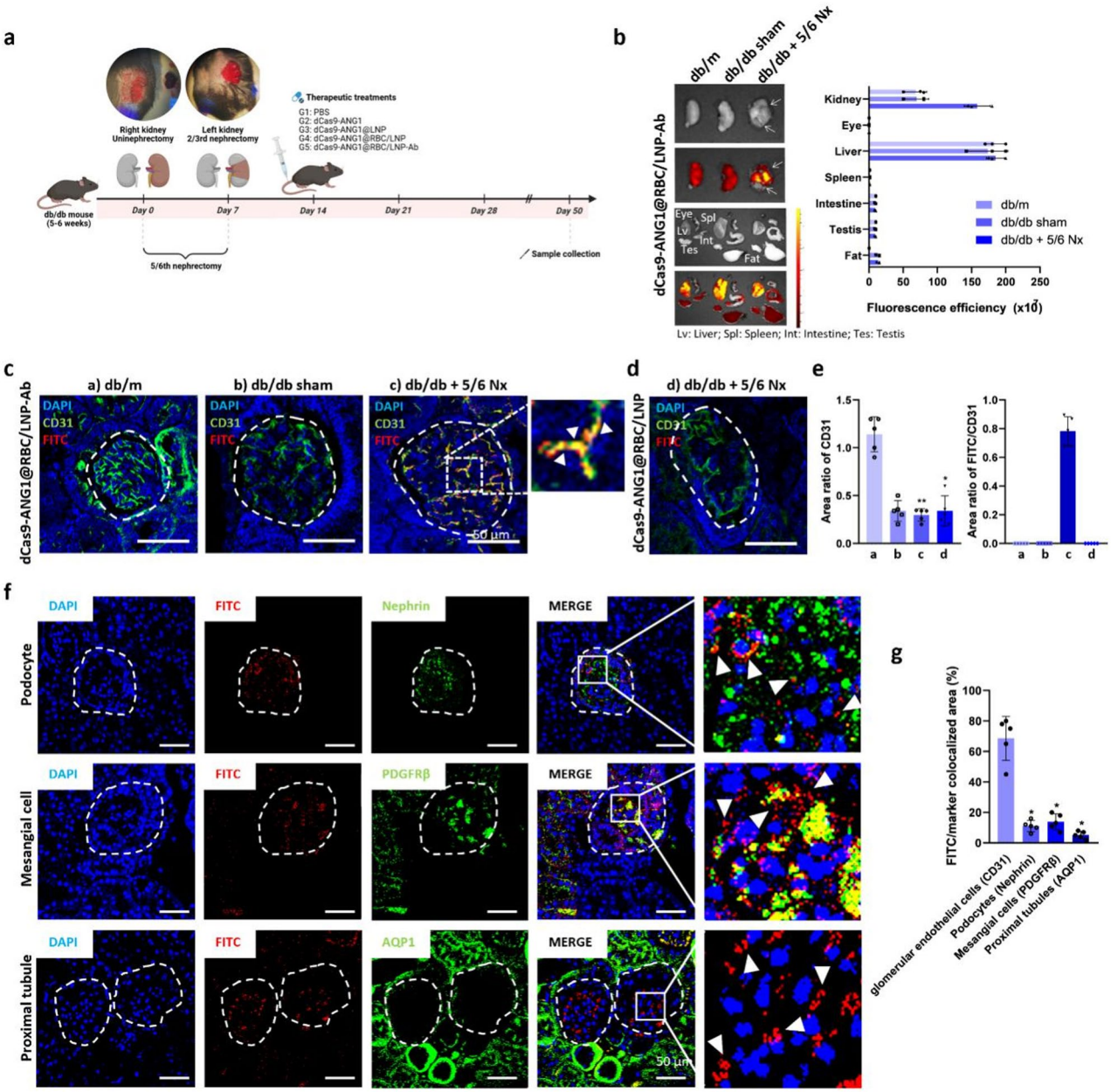


Fig. 4 Glomerular targeting of the nanoparticle in DKD mice. (**a**) Schematic overview of the experimental design, including induction of advanced DKD in db/db mice by 5/6 Nx, systemic nanoparticle administration, and subsequent in vivo and molecular analyses. (**b**) Whole-body and ex vivo fluorescence imaging showing biodistribution and preferential kidney accumulation of dCas9-ANG1@RBC/LNP-Ab at 2 h post-injection. (**c**, **d**) Representative immunofluorescence images showing localization of FITC-labeled VE-PTP-targeted nanoparticles (c) and non-antibody-conjugated nanoparticles (d) within CD31-positive GECs in glomerular structures. (e) Quantification of FITC-labeled nanoparticle signal within CD31-positive glomerular endothelial regions. (**f**) Representative confocal images showing FITC-labeled nanoparticle localization relative to nephrin-positive podocytes, PDGFRβ-positive mesangial cells, and AQP1-positive proximal tubules in kidney sections from db/db + 5/6 Nx mice. Dashed lines indicate glomerular regions, and arrowheads indicate FITC-positive nanoparticle signals. (**g**) Quantification of FITC/marker colocalized area for CD31, nephrin, PDGFRβ and AQP1. All in vivo experiments were performed with $n = 10$ mice per group. Data are presented as mean ± SD; $^{*}p < 0.05$. Figure 4a was created with BioRender.com

https://doi.org/10.1186/s12951-026-05042-5

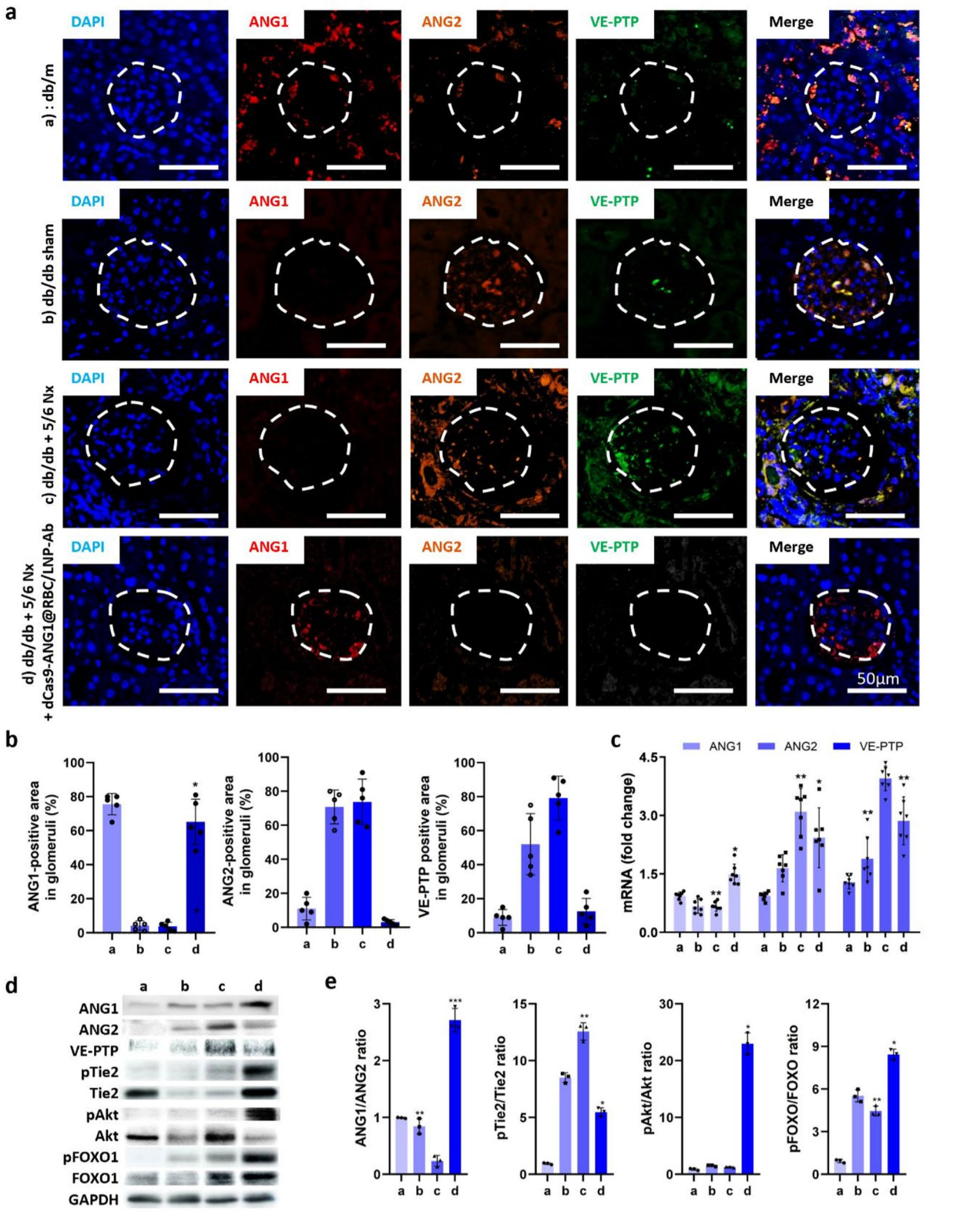


Fig. 5 Glomerular restoration of ANG1-Tie2 signaling in DKD mice. (**a**) Confocal images of kidney sections stained for ANG1 (red), ANG2 (orange), and VE-PTP (green) in db/m, db/db sham, db/db 5/6 Nx, and db/db 5/6 Nx + dCas9-ANG1@RBC/LNP-Ab groups. (**b**) Quantification of ANG1, ANG2, VE-PTP-positive area in glomeruli. (**c**) RT-qPCR analysis of *Ang1*, *Ang2*, and *Ve-ptp* mRNA expression levels in kidney tissues. (**d**, **e**) Western blot analysis and corresponding quantification of the ANG1-Tie2-Akt signaling cascade and FOXO1 phosphorylation in kidney tissues. Data are presented as mean ± SD ($n = 5$); *$p < 0.05$, **$p < 0.01$, ***$p < 0.001$

To confirm that the in vivo effects were dependent on ANG1-specific CRISPR activation rather than nonspecific effects of the nanoparticle carrier, antibody conjugation, or dCas9 protein, we included additional CRISPRa control groups. Free dCas9-ANG1 RNP, dCas9-only@RBC/LNP-Ab, dCas9-scrambled sgRNA@RBC/LNP-Ab, and dCas9-ANG1@RBC/LNP-IgG showed limited ANG1 activation compared with the VE-PTP-targeted dCas9-ANG1@RBC/LNP-Ab formulation (Additional file 1: Figure S11). Notably, the IgG-conjugated control showed limited glomerular localization, and the scrambled sgRNA control did not induce ANG1 expression. These findings support that ANG1 upregulation was mediated by ANG1-targeted sgRNA-dependent CRISPRa rather than nonspecific effects of the delivery platform. Because dCas9-VP64 functions as a transcriptional activator, we evaluated potential off-target transcriptional activation using targeted qPCR. Predicted off-target-associated genes were selected based on CRISPOR analysis of the ANG1-targeting sgRNA sequence. The expression of GOLGA8S, SCRT2, and SLC52A3 was not increased by dCas9-ANG1@RBC/LNP-Ab compared with DKD control or CRISPRa control groups (Additional file 1: Figure S12a, b). We also examined representative endothelial activation, inflammatory, angiogenic, and fibrosis-related genes, including ICAM1, IL6, VEGFA, and TGFB1 (Additional file 1: Figure S12c). The control formulations did not markedly affect the expression of the examined safety-related genes. In contrast, the final dCas9-ANG1@RBC/LNP-Ab formulation tended to restore DKD-induced changes in IL6, VEGFA, and TGFB1 toward normal levels, with only a modest change in ICAM1. These findings support that the final formulation did not cause broad off-target transcriptional activation, but rather promoted partial normalization of DKD-associated gene expression.

Collectively, these data indicate that VE-PTP-targeted delivery of dCas9-ANG1 reactivated the ANG1-Tie2-Akt signaling cascade in vivo, reversing endothelial signaling defects characteristic of advanced diabetic kidney injury. These findings support the concept that biomimetic RBC-hybrid nanoparticles can be combined with antibody-mediated targeting to improve cell-specific gene modulation within the diabetic glomerular microenvironment.

dCas9-ANG1@RBC/LNP-Ab ameliorates kidney dysfunction in db/db 5/6 Nx mice

We next examined whether ANG1 reactivation translated into functional and structural kidney protection in vivo. db/db 5/6 Nx mice exhibited progressive weight decline and reduced survival compared with db/m controls, reflecting severe systemic and kidney deterioration (Fig. 6a, b). Treatment with dCas9-ANG1@RBC/LNP-Ab partially stabilized body weight and improved survival rates, suggesting an overall protective effect in advanced diabetic kidney injury. Kidney functional parameters were markedly impaired in db/db 5/6 Nx mice, as evidenced by substantial increases in urinary albumin-to-creatinine ratio (uACR) and elevated blood urea nitrogen (BUN) levels (Fig. 6c, d). Administration of dCas9-ANG1@RBC/LNP-Ab significantly reduced both uACR and BUN compared with untreated db/db 5/6 Nx mice, indicating improved glomerular filtration barrier integrity and kidney function.

Histological evaluation corroborated the severe glomerular pathology observed in db/db 5/6 Nx mice. H&E and PAS staining revealed pronounced glomerular hypertrophy and excessive mesangial matrix expansion, while Masson's trichrome staining demonstrated extensive fibrotic remodeling within the glomeruli (Fig. 6e). Notably, administration of dCas9-ANG1@RBC/LNP-Ab markedly attenuated these structural abnormalities, restoring glomerular architecture and significantly reducing mesangial and fibrotic lesions. Quantitative morphometric analysis confirmed a significant reduction in glomerular volume and mesangial expansion percentage in treated

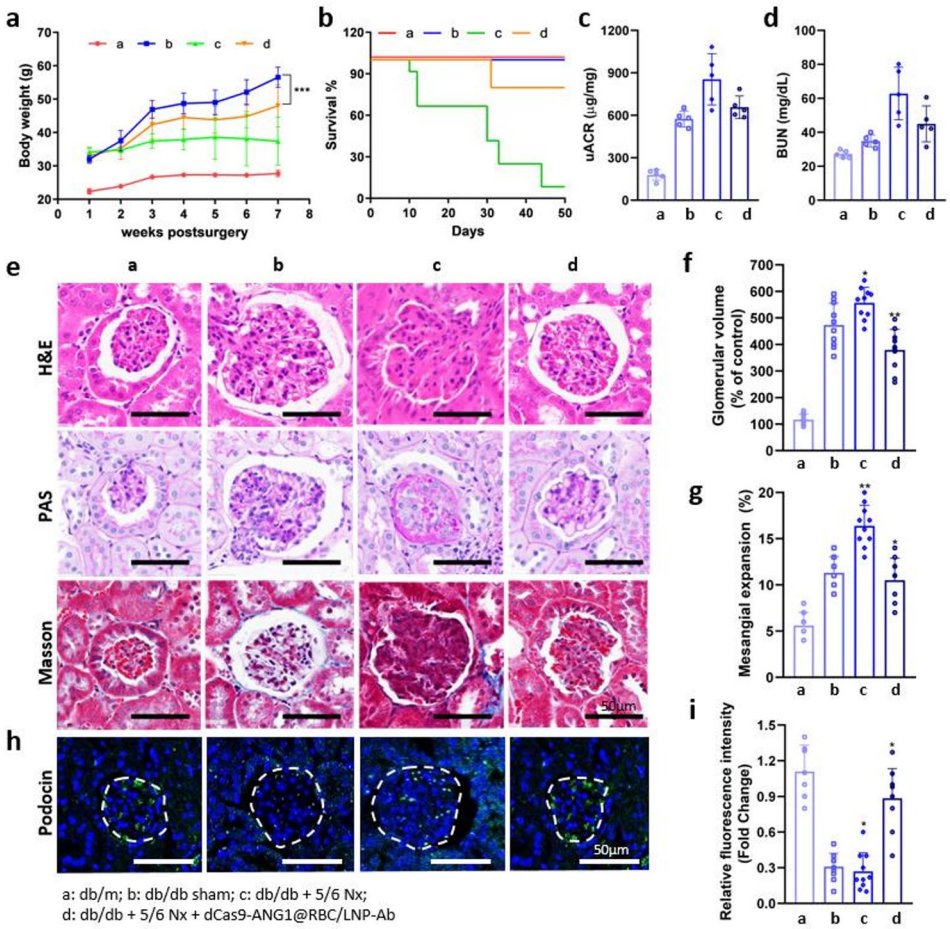


Fig. 6 Effects of dCas9-ANG1@RBC/LNP-Ab on kidney function and structural injury in DKD mice. (**a**, **b**) Longitudinal monitoring of body weight and survival over the 7-week experimental period. (**c**, **d**) Kidney functional assessment based on urinary albumin-to-creatinine ratio (uACR) and blood urea nitrogen (BUN) levels ($n = 5$ per group). (**e**) Representative kidney histology images stained with H&E, PAS, and Masson's trichrome showing glomerular hypertrophy, mesangial expansion, and fibrotic remodeling. (**f**, **g**) Quantitative morphometric analysis of glomerular volume and mesangial expansion area using ImageJ. (**h**, **i**) Immunofluorescence staining and quantification of podocin (green) to assess podocyte integrity. Data are presented as mean ± SD. *$p < 0.05$, **$p < 0.01$, ***$p < 0.001$

mice compared with untreated db/db 5/6 Nx controls (Fig. 6f, g). These findings indicate that restoration of endothelial ANG1 signaling mitigates glomerular remodeling and matrix accumulation in advanced DKD. Importantly, endothelial-directed ANG1 activation also exerted protective effects on podocytes. Immunofluorescence staining for podocin revealed marked loss and reduced fluorescence intensity in db/db 5/6 Nx mice, consistent with podocyte injury and detachment (Fig. 6h, i). Treatment with dCas9-ANG1@RBC/LNP-Ab significantly restored podocin expression, indicating preservation of podocyte integrity. These results suggest that endothelial ANG1 reactivation not only stabilizes endothelial signaling but also confers secondary protection to adjacent podocytes within the glomerular microenvironment.

To assess systemic safety, major organs, including the liver, spleen, testis and intestine were subjected to H&E staining. No obvious histopathological abnormalities, inflammatory infiltration, or structural damage were observed in the treatment group compared with controls, indicating that dCas9-ANG1@RBC/LNP-Ab did not induce detectable treatment-associated toxicity in major non-kidney tissues (Additional file 1: Figure S13a). To further assess systemic tolerability, we expanded the safety evaluation by measuring serum chemistry markers. dCas9-ANG1@RBC/LNP-Ab treatment did not further increase liver-associated injury markers, including aspartate aminotransferase (AST), alanine aminotransferase (ALT) and alkaline phosphatase (ALP), compared with untreated db/db + 5/6 Nx mice. In addition, tissue injury markers, including creatine phosphokinase (CPK) and lactate dehydrogenase (LDH), were not elevated after treatment and were reduced compared with untreated db/db + 5/6 Nx controls (Additional file 1: Figure S13b, c). Together with H&E staining of major organs, these findings support the short-term systemic tolerability of dCas9-ANG1@RBC/LNP-Ab under the tested conditions.

Collectively, these data demonstrate that VE-PTP-targeted dCas9-ANG1 delivery reestablishes ANG1-Tie2 signaling in vivo and translates into functional, structural, and cellular protection in advanced DKD. From a nanotherapeutic perspective, these results show that biomimetic RBC-hybrid nanoparticles can deliver CRISPRa RNPs to a disease-relevant endothelial compartment after systemic administration and produce measurable therapeutic effects. Although further studies are needed to optimize dosing, long-term safety, repeated administration, and manufacturing scalability, this platform provides proof-of-concept for targeted endothelial gene modulation in microvascular kidney disease.

Discussion

A key finding of this study is that disease-associated VE-PTP upregulation can be leveraged as a molecular entry point for targeting injured glomerular endothelium. VE-PTP has traditionally been viewed as a negative regulator of Tie2 signaling and a contributor to endothelial destabilization. Here, we repurposed this disease-induced endothelial marker to direct CRISPRa RNP delivery to dysfunctional GECs. This pathology-guided strategy enabled preferential glomerular endothelial localization and kidney-preferential functional ANG1 activation, despite transient hepatic nanoparticle accumulation after systemic administration [25, 26]. These findings suggest that functional gene activation depends not only on initial biodistribution but also on disease-associated cellular uptake and intracellular target engagement.

The use of CRISPR activation further distinguishes this strategy from conventional genome-editing approaches. Because CRISPRa modulates transcription without inducing DNA double-strand breaks, it enables upregulation of endogenous genes without permanent genomic modification. Delivery in RNP format may further limit intracellular persistence, providing temporal control of gene activation and potentially reducing risks associated with prolonged exposure. In this setting, the RBC membrane-hybrid delivery system served as a biomimetic vehicle to improve vascular compatibility while supporting endothelial-directed delivery of the CRISPRa payload. This platform also differs from existing endothelial-targeted nanoparticle and Tie2-directed therapeutic strategies. Many endothelial-targeted nanoparticles use broadly expressed endothelial markers or adhesion molecules, whereas our approach exploits disease-associated VE-PTP upregulation to target dysfunctional glomerular endothelial cells. Compared with conventional LNP delivery systems, which frequently exhibit prominent hepatic accumulation after systemic administration, VE-PTP antibody functionalization of RBC-hybrid LNPs supported preferential glomerular endothelial localization and kidney-preferential functional ANG1 activation. In addition, unlike direct VE-PTP inhibition or exogenous angiopoietin-based therapies, dCas9-ANG1@RBC/LNP-Ab activates endogenous ANG1 expression in target endothelial cells, thereby restoring ANG1-Tie2-Akt signaling through transcriptional modulation.

Several limitations should be acknowledged. First, although the db/db 5/6 nephrectomy model reflects features of advanced DKD, it does not fully recapitulate the heterogeneity of human disease. Validation in additional DKD models and human kidney tissues will be important. Second, although dCas9-ANG1@RBC/LNP-Ab showed kidney-preferential functional ANG1 activation, early nanoparticle accumulation in off-target organs such as the liver was observed. Further optimization will be needed to reduce extra-kidney clearance and improve glomerular endothelial delivery efficiency. Third, although short-term systemic tolerability was supported after single-dose administration, repeated-dose safety, long-term biodistribution, complement activation, inflammatory cytokine responses, and adaptive immune responses against Cas9, RBC membrane components, PEG, or the targeting antibody were not comprehensively assessed. Finally, the durability of gene activation and scalability of RBC-hybrid nanoparticle manufacturing require further evaluation before clinical translation.

Overall, these findings establish a biomimetic RBC membrane-hybrid nanoparticle strategy for endothelial CRISPRa RNP delivery in DKD. By linking disease-associated endothelial targeting with endogenous therapeutic gene activation, this platform provides a framework for precision modulation of glomerular microvascular dysfunction.

Conclusions

In this study, we developed a VE-PTP-targeted biomimetic RBC membrane-hybrid lipid nanoparticle platform for glomerular endothelial delivery of dCas9-based CRISPRa RNPs. By combining ionizable lipid-mediated RNP loading, RBC membrane-derived biomimicry, and antibody-mediated endothelial targeting, this platform enabled delivery of CRISPRa components to injured GECs and reactivation of endogenous ANG1 expression in DKD. Targeted ANG1 activation restored ANG1-Tie2 signaling, improved glomerular barrier integrity, reduced albuminuria, and attenuated structural kidney injury in advanced DKD mice. These findings support biomimetic endothelial-targeted CRISPRa delivery as a potential therapeutic strategy for diabetic kidney disease.

Abbreviations

ANG1	angiopoietin-1
ANG2	angiopoietin-2
BUN	blood urea nitrogen
CD31	cluster of differentiation 31
CD47	cluster of differentiation 47
CLSM	confocal laser scanning microscopy
CRISPRa	CRISPR activation
dCas9	nuclease-deficient CRISPR-associated protein 9
DKD	diabetic kidney disease
DLS	dynamic light scattering
EDC	1-ethyl-3-(3-dimethylaminopropyl) carbodiimide
GECs	glomerular endothelial cells
HG	high glucose
HIF1α	hypoxia-inducible factor 1 alpha
LNP	lipid nanoparticle
NHS	N-hydroxysuccinimide
PBS	phosphate-buffered saline
PEG	polyethylene glycol
RBC	red blood cell
RNP	ribonucleoprotein
RT-qPCR	reverse transcription quantitative polymerase chain reaction
sgRNA	single-guide RNA
TEM	transmission electron microscopy
Tie2	TEK receptor tyrosine kinase
uACR	urinary albumin-to-creatinine ratio
VE-PTP	vascular endothelial protein tyrosine phosphatase

Supplementary Information The online version contains supplementary material available at https://doi.org/10.1186/s12951-026-05042-5.

Acknowledgements Not applicable.

Author contributions J.-Y.R., G.W.B. and N.J.S. contributed equally to this work. J.-Y.R. and G.W.B. designed and synthesized the nanoparticles, performed physicochemical characterization, and conducted the in vitro and in vivo experiments. N.J.S. contributed to data analysis, interpretation of results, and manuscript drafting and revision. I.R., J.L. and A.K. contributed to data acquisition and experimental support. S.P. and D.K.K. conceived and supervised the study, interpreted the data, and wrote the final manuscript. All authors discussed the results and contributed to the revision of the final manuscript.

Funding This work was supported by grants from the Korea Health Technology R&D Project through the Korea Health Industry Development Institute (KHIDI), funded by the Ministry of Health and Welfare, Republic of Korea (No. RS-2025-02215568 and No. RS-2025-25459535). This research utilized the Pathology Core Facility at the Center for Medical Innovation (CMI), Seoul National University Hospital (SNUH). The Biobank of Seoul National University Hospital (Korea Biobank Network, project No. 2024ER050800) is acknowledged.

Data availability No datasets were generated or analysed during the current study.

Declarations

Ethics approval and consent to participate All experiments were performed in accordance with the Animal Welfare Regulations and SNUH IACUC guidelines. Animal experiments were carried out according to the animal experiment procedure approved by the Institutional Animal Care and Use Committee of Seoul National University Hospital (SNUH) (No. 25-0100-S1A0).

Consent for publication Not applicable.

Competing interests The authors declare no competing interests.

Open Access This article is licensed under a Creative Commons Attribution-NonCommercial-NoDerivatives 4.0 International License, which permits any non-commercial use, sharing, distribution and reproduction in any medium or format, as long as you give appropriate credit to the original author(s) and the source, provide a link to the Creative Commons licence, and indicate if you modified the licensed material. You do not have permission under this licence to share adapted material derived from this article or parts of it. The images or other third party material in this article are included in the article's Creative Commons licence, unless indicated otherwise in a credit line to the material. If material is not included in the article's Creative Commons licence and your intended use is not permitted by statutory regulation or exceeds the permitted use, you will need to obtain permission directly from the copyright holder. To view a copy of this licence, visit http://creativecommons.org/licenses/by-nc-nd/4.0/.

References

1. Kim DH, Hyun YY, Cha JJ, Lee S, Lee HK, Choi JW, et al. Kidney Health Plan 2033 in Korea: bridging the gap between the present and the future. Kidney Res Clin Pract. 2024;43(1):8–19.
2. de Boer IH, Khunti K, Sadusky T, Tuttle KR, Neumiller JJ, Rhee CM, et al. Diabetes Management in Chronic Kidney Disease: A Consensus Report by the American Diabetes Association (ADA) and Kidney Disease: Improving Global Outcomes (KDIGO). Diabetes Care. 2022;45(12):3075–90.
3. Min L, Chen Y, Liu R, Li Z, Gu L, Mallipattu S, et al. Targeting Kruppel-Like Factor 2 as a Novel Therapy for Glomerular Endothelial Cell Injury in Diabetic Kidney Disease. J Am Soc Nephrol. 2025;36(2):193–204.
4. Yu L, Ekperikpe US, Korsmo HW, Zhao S, Yi Z, Haydak J, et al. Podocyte-derived endothelin-1 and endothelial cell endothelin A receptors are essential for glomerular injury in mouse models of focal segmental glomerulosclerosis. Kidney Int. 2026;109(5):971–86.
5. Yang J, Liu Z. Mechanistic Pathogenesis of Endothelial Dysfunction in Diabetic Nephropathy and Retinopathy. Front Endocrinol (Lausanne). 2022;13:816400.
6. Onetti Muda A, Feriozzi S, Crescenzi A, Faraggiana T. Role of endothelial cells in the development of glomerular lesions of mesangiocapillary glomerulonephritis. J Pathol. 1995;177(3):269–74.
7. Brenner JS, Pan DC, Myerson JW, Marcos-Contreras OA, Villa CH, Patel P, et al. Red blood cell-hitchhiking boosts delivery of nanocarriers to chosen organs by orders of magnitude. Nat Commun. 2018;9(1):2684.
8. Villa CH, Pan DC, Zaitsev S, Cines DB, Siegel DL, Muzykantov VR. Delivery of drugs bound to erythrocytes: new avenues for an old intravascular carrier. Ther Deliv. 2015;6(7):795–826.
9. Mukai H, Ogawa K, Kato N, Kawakami S. Recent advances in lipid nanoparticles for delivery of nucleic acid, mRNA, and gene editing-based therapeutics. Drug Metab Pharmacokinet. 2022;44:100450.
10. Wan Y, Li C, Fu LH, Feng T, Zhang Y, Li Y, et al. Erythrocyte Membrane Camouflaged Nanotheranostics for Optical Molecular Imaging-Escorted Self-Oxygenation Photodynamic Therapy. Small. 2024;20(31):e2309026.
11. Shen J, Frye M, Lee BL, Reinardy JL, McClung JM, Ding K, et al. Targeting VE-PTP activates TIE2 and stabilizes the ocular vasculature. J Clin Invest. 2014;124(10):4564–76.

12. Carota IA, Kenig-Kozlovsky Y, Onay T, Scott R, Thomson BR, Souma T, et al. Targeting VE-PTP phosphatase protects the kidney from diabetic injury. J Exp Med. 2019;216(4):936–49.
13. Luo AJ, Chang FC, Lin SL. Exploring Angiopoietin-2: Clinical Insights and Experimental Perspectives in Kidney Diseases. Kidney Int Rep. 2024;9(12):3375–85.
14. Pietila R, Marks-Hultstrom A, He L, Nanavazadeh S, Quaggin SE, Betsholtz C et al. TIE2 activation by antibody-clustered endogenous angiopoietin-2 prevents capillary loss and fibrosis in experimental kidney disease. J Clin Invest. 2025;135(21).
15. Li Y, Liu P, Zhou Y, Maekawa H, Silva JB, Ansari MJ, et al. Activation of Angiopoietin-Tie2 Signaling Protects the Kidney from Ischemic Injury by Modulation of Endothelial-Specific Pathways. J Am Soc Nephrol. 2023;34(6):969–87.
16. Robinson-Cohen C, Katz R, Price BL, Harju-Baker S, Mikacenic C, Himmelfarb J, et al. Association of markers of endothelial dysregulation Ang1 and Ang2 with acute kidney injury in critically ill patients. Crit Care. 2016;20(1):207.
17. Ma X, Lu YP, Yang L, Song J, Luo GH, Shi YJ, et al. Rapamycin and cyclosporine have different effects on expression of Ang-1 and Ang-2 and Tie2 in rat renal allograft with chronic allograft nephropathy. Transpl Proc. 2008;40(8):2804–7.
18. Labun K, Montague TG, Krause M, Torres Cleuren YN, Tjeldnes H, Valen E. CHOPCHOP v3: expanding the CRISPR web toolbox beyond genome editing. Nucleic Acids Res. 2019;47(W1):W171–4.
19. Haeussler M, Schönig K, Eckert H, et al. Evaluation of off-target and on-target scoring algorithms and integration into the guide RNA selection tool CRISPOR. Genome Biol. 2016;17:148.
20. Cho EY, Ryu JY, Lee HAR, Hong SH, Park HS, Hong KS, Park SG, et al. Lecithin nano-liposomal particle as a CRISPR/Cas9 complex delivery system for treating type 2 diabetes. J Nanobiotechnol. 2019;17:19.
21. Ryu JY, Won EJ, Lee HAR, Kim JH, Hui E, Kim HP, Yoon TJ. Ultrasound-activated particles as CRISPR/Cas9 delivery system for androgenic alopecia therapy. Biomaterials. 2020;232:119736.
22. Hu CM, Fang RH, Luk BT, Chen KN, Carpenter C, Gao W, et al. Marker-of-self' functionalization of nanoscale particles through a top-down cellular membrane coating approach. Nanoscale. 2013;5(7):2664–8.
23. Brosius FC 3rd, Alpers CE, Bottinger EP, Breyer MD, Coffman TM, Gurley SB, et al. Mouse models of diabetic nephropathy. J Am Soc Nephrol. 2009;20(12):2503–12.
24. Chow BSM, Allen TJ. Mouse Models for Studying Diabetic Nephropathy. Curr Protoc Mouse Biol. 2015;5(2):85–94.
25. Yuan Z, Luozhong S, Li R, Gu W, Chen Y, Bhashyam D, et al. Transient Macrophage Depletion Circumvents Scavenging and Redirects Biodistribution of mRNA-Lipid Nanoparticles. ACS Nano. 2025;19(14):14422–33.
26. Witzigmann D, Kulkarni JA, Leung J, Chen S, Cullis PR, van der Meel R. Lipid nanoparticle technology for therapeutic gene regulation in the liver. Adv Drug Deliv Rev. 2020;159:344–63.

Publisher's note Springer Nature remains neutral with regard to jurisdictional claims in published maps and institutional affiliations.

Authors and Affiliations

Jee-Yeon Ryu[1,2] · Geon Woo Baek[3] · Nicholas J. Steers[4] · Ilhwan Ryu[5] · Jinsun Lee[1] · Ara Ko[1] · Sehoon Park[1] · Dong Ki Kim[1,3,6]

✉ Sehoon Park
ofsehoon@gmail.com

✉ Dong Ki Kim
dkkim73@gmail.com

[1] Department of Internal Medicine, Seoul National University Hospital, Seoul 03080, South Korea

[2] Center for Medical Innovation, Biomedical Research Institute, Seoul National University Hospital, Seoul 03082, South Korea

[3] Department of Translational Medicine, College of Medicine, Seoul National University, Seoul 03080, South Korea

[4] Department of Medicine, Division of Nephrology, Irving Medical Center, College of Physicians and Surgeons, Columbia University, New York, NY 10032, USA

[5] Cooperative Center for Research Facilities, Kookmin University, Seoul 02707, South Korea

[6] Biomedical Research Institute, Seoul National University Human Biobank, Seoul National University Hospital, Seoul 02707, South Korea